RSC Advances

ROYAL SOCIETY OF CHEMISTRY

www.rsc.org/advances

Aminosilane-functionalization of a nanoporous Y-type zeolite for application in a cellulose acetate based mixed matrix membrane for CO_2 separation

Hamidreza Sanaeepur[1], Ali Kargari[1], Bahram Nasernejad[2,*]

1- Membrane Processes Research Laboratory (MPRL), Petrochemical Engineering Department, Amirkabir University of Technology (Tehran Polytechnic), Mahshahr Campus, Mahshahr, P.O. Box 415, Iran.

2- Chemical Engineering Department, Amirkabir University of Technology (Tehran Polytechnic), Hafez Ave., P.O. Box 15875-4413, Tehran, Iran.

[*]Corresponding author: Tel: + 98 (21) 64543128; fax: +98 (21) 66414213,
E-mail: Banana@aut.ac.ir

Abstract

The purpose of this study is the surface modification of a micro-sized nanoporous zeolite through the silylation reaction and incorporating the silylated particles into a homogeneous cellulose acetate (CA) membrane to achieve better polymer-zeolite adhesion in the corresponding mixed matrix membranes (MMMs). In the current study, 3-aminopropyl(diethoxy)methylsilane (APDEMS) is used as the silane coupling agent and micro-sized nanoporous sodium zeolite-Y (Na-Y) as the precursor zeolite. Unmodified pure form of the zeolite (Na-Y), the silanated zeolite (NaY-sm) and the corresponding MMMs were characterized using the DLS, BET, FTIR-ATR, XRD, SEM, and TG/DSC analyses. Moreover, the CO_2/N_2 separation performances of the prepared membranes were evaluated through the gas permeation measurements. The results demonstrated that this modification results in an increase in average particle diameter, external surface area, and overall volume (or size) as well as a decrease in the micropore surface areas and volumes and also the crystallinity of the resultant modified zeolite particles. In addition, it led to an improvement in the uniformity of the particle distributions all over the MMM structure, and a considerable reduction in the numbers/sizes of the undesirable cracks and agglomerates. The CO_2 permeability of CA increased about 77.55 % at 4 bar for the CA/NaY-sm 20 wt.% membrane. This is while that not only the CO_2 permeability of CA/NaY-sm membranes was not reduced as compared to CA/NaY ones, but also it was shown an averaged 4.67 % increase, too. Moreover, an average CO_2/N_2 selectivity of 6.34 % was obtained for NaY-sm filled MMMs compared to those filled with the pure NaY ($\geq$ 4 bar). This can be a proper contribution to developing new materials in the field.

Keywords: Mixed matrix membrane, Zeolite, Silane coupling agent, Surface modification, CO_2 separation.

1. Introduction

Carbon dioxide (CO_2) is the most abundant greenhouse gas (GHG) in the atmosphere that is mainly emitted by the industrial sectors.[1] Membrane gas separation is proposed as emerging technology for CO_2 capture and storage (CCS).[2, 3] High performance gas separation membranes can be fabricated by incorporating inorganic fillers into the polymeric membranes to form the mixed matrix membranes (MMMs). Zeolite-filled MMMs have the potential to achieve superior separation performance with equal or greater fluxes compared to existing polymer membranes while maintaining their advantages.[4, 5] However, the most common problem of non-selective "void", due to a poor interaction or de-wetting of the polymer chains and external surface of the zeolite at the interface between them, can result in a degradation of the MMM performances.[6]

Up to now, different strategies have been considered for achieving better polymer-zeolite adhesion in zeolite-filled mixed matrix membranes (MMMs) for gas separation, such as: (a) chemical treatment (mainly silanation reaction) of the zeolite surface using different organic functional groups (silane coupling agents),[7] (b) creating a nanoscopic inorganic whisker-like or roughened structure (through the five routes of halide/Grignard decomposition reaction, solvothermal deposition, modified solvothermal depositions, ion exchange induced surface crystallization, and epitaxial surface growth) on the outer zeolite surfaces,[8-10] (c) surface-initiated polymerization with preformed zeolites,[9] (d) in situ synthesis of zeolites within prefabricated polymer matrixes,[11] (e) annealing the membranes above the glass transition temperature of the polymer,[11, 12] or (f) adding plasticizer and/or antiplasticizer additives into the membrane formulation.[13] Furthermore, a few works were subjected to introducing the concept of zeolite-filled porous MMMs and their potential use for gas separations.[14, 15] This resulted in an increase in permeation performance but an undesirable decrease in selectivity compared with the dense MMMs.

Silane coupling agents have a general formula of R_nSiX_{4-n} (R: the functional organic group, X: an easily hydrolysable group such as methoxy, ethoxy or acetoxy).[16, 17] When they are hydrolyzed to silanols, $R_nSi(OH)_{4-n}$, it possibly reacts with hydroxyl groups on the zeolite surface, and amino groups or other functional groups in the polymer matrix to enhance the compatibility between the phase boundaries.[18-20] Amino-, vinyl-, and acrylsilane modified zeolites are some of the new opportunities of MMM materials.[21] A unique feature of zeolites modification by aminosilanes is their high capacity for adsorption of CO_2 as well as higher CO_2/N_2 selectivity at low partial pressures, due to preferential reactions with CO_2.[22] Aminosilanes, as a particular type of organosilanes, contain primary, secondary, and tertiary amines. They have a hydrolytically sensitive center that can react with hydroxyl groups (or silanols) of zeolite surface to form a silylated surface where the silicon is covalently bonded to the surface via an oxygen atom (organic-modification of silanols).[23-25] The covalent bonds formed through the hydrolysis and condensation reactions between the organosilane and the zeolite surface in a polar medium remove the surface silanol groups and make the surface hydrophobic.[18] The most prominent types of aminosilane coupling agents are γ-aminopropyltriethoxysilane (APTES), N-β-aminoethyl-γ-aminopropyltrimethoxysilane, γ-glycidyloxypropyltrimethoxysilane, 3-aminopropyldimethylethoxysilane (APDMES) or 3-aminopropyldiethoxymethylsilane (APDEMS).[26] The NH groups on the surface of the modified zeolite could react with the polar carbonyl (−CO) and oxycarbonyl (−COO) groups of cellulose acetate (CA) through an acid-base ionic interaction.

A more commonly cited silane coupling agent in the literatures is APDEMS, with two alkoxy groups. It has two ethoxy (CH_3CH_2O) groups and an additional hydrophobic group (CH_3) and compared to APTES with three ethoxy groups may lower the number of coupling points with the zeolite surface during the silanization reaction.[27] The presence of APDEMS introduces an approximately 5–9 Å gap between polymer chains and zeolite surface and thus

decreases the negative effect of partial pore blockage of zeolites by polymer chains, and also, its subsequent effect of polymer chain rigidification.[28] Clarizia *et al*.[29] incorporated a very high loading of 30 wt.% NaA zeolite (the mean value of about 3.0 μm and Si/Al ratio of equal to 1.0) modified with APDEMS, diethanolamine (DEA) and Poly-α-pinene (PαP) into modified polyetheretherketone (PEEK-WC). Comparing the three coupling agents at high loading close to the percolation threshold, they concluded that DEA, being the smallest coupling agent, was more effective to reduce the void between the zeolite and the polymer. They demonstrated that it most likely achieved better results at lower zeolite contents (for example in a MMM containing 10 wt.% PαP as additive). Unfortunately, they have not reported the effect of other coupling agents in low zeolite contents. In another work, according to the same BET results of surface area and total pore volume of zeolites 3A, 4A and 5A before and after modification with APDEMS, Li *et al*.[30] demonstrated that the micropore of zeolites is not influenced by the addition of APDEMS. Moreover, they showed that MMMs made from incorporating the modified-zeolites into polyethersulfone (PES) matrix have both CO_2 permeability and selectivity higher than those of MMMs with unmodified-zeolites at 20 wt.% loading. Similar to Chung *et al*.[28] they also attributed the results to a 5–9 Å distance between polymer chains and zeolite surfaces made by APDEMS which decreases the degree of the partial pore blockage of the zeolites by polymer chains. In a critical review, Basu *et al*.[31] stated that the presence of larger pore sizes in zeolites (13X in comparison with 3A, 4A, 5A) result in facilitated movement of the gas molecules and hence increase the permeability. In addition, a further modification with silane coupling agents results in the selectivity increase.

This paper contains a design method for incorporating an aminosilane-functionalized NaY zeolite with – large pore sizes and – enhanced CO_2 sorption property into the commercial CA membrane material to form new MMMs in order to investigate their performance for post-

combustion carbon capture (the CO_2/N_2 separation). To the best of our knowledge, the so-called membranes are prepared and tested for the first time. A very commonly used aminosilane coupling agent, APDEMS, is chosen for zeolite modification. In addition, a simple method of fabricating a dense membrane is also chosen for preparing the MMMs.

2. Experimental

2.1. Materials

Cellulose acetate (CA), average Mn ~30,000 by GPC, with acetyl content 39.8 wt.% and bulk density of 1.3 g/mL at 25 °C was acquired from Sigma-Aldrich® (Saint Louis, MO, USA). Sodium Y zeolite (NaY) powder was also supplied by Sigma-Aldrich® (Saint Louis, MO, USA). Aminosilane coupling agent, 3-aminopropyl(diethoxy)methylsilane 97%, APDEMS, with boiling point 85-88 °C/8 mmHg and density of 0.916 g/mL at 25 °C, was also purchased from Sigma-Aldrich® (Saint Louis, MO, USA). Analytical grade tetrahydrofuran (THF) and ethanol were acquired from Merck (Darmstadt, Germany) and used as such without further purification. All the gases having 99.999% purity were purchased from Technical Gases Ltd. supplied by Oxygen Yaran Company, Mahshahr, Iran.

2.2. Grafting the zeolites

2 g dried zeolite powder was suspended in 100 ml ethanol (as a polar medium) and stirred in a glass round bottom flask for 1 h at 80 °C. 8 ml APDEMS (4 ml aminosilane/g zeolite) as the grafting agent was then added dropwise to the mixture under stirring using a precision syringe. After the completion of the reaction (24 h), the mixture was then cooled to room temperature, filtered and washed with ethanol several times. Finally, the grafted or silane-modified zeolites were dried in a vacuum oven at 100 °C overnight. A proposed schematic of the grafting reaction between APDEMS and the zeolite surface is illustrated in Figure 1.

2.3. Membrane preparation

THF was chosen as the solvent for CA because of its sufficient evaporation rate to quick formation of a uniform polymer-particle composite after casting on a glass plate. The CA polymer was dried overnight at 80 °C in an oven before use. The NaY powder was also dried overnight at 100 °C in an oven that was followed by further drying for two-days at 120 °C in a vacuum oven before use. A predetermined amount of NaY-sm and CA in THF solvent (15 wt.% solution) was well mixed through the following procedure. First, a certain amount (e.g., 0.150 g for CA/NaY-sm 5 wt.%) of NaY-sm powder was added to 8.5 g of THF in a 100 ml round glass bottle with a plastic sealing cap and was stirred for 24 h at room temperature. Then, about 10 % of the total CA (e.g., 0.135 g of 1.350 CA for CA/NaY-sm 5 wt.%) was added to the NaY-sm/THF suspension and further stirred for 4 h. This is done to readily form an organic thin layer made by CA chains (in a dilute and less viscose solution) around the solid NaY-sm particles. Next, the remaining second part of CA was added to the mixture and mixed entirely for 6 h which takes the advantage from more organic-organic compatibility with the previously formed CA layer. Finally, it was filtered and degassed for about an hour at room temperature and spread onto a clean glass plate with a doctor's blade with a 300 μm gap. After a day of solvent evaporation the membrane was detached from the plate and placed in a 150 °C vacuum oven for 48 h by special care in slow initial heating and final cooling rates. The final membrane thicknesses were measured by a digital micrometer (Mitutoyo®, Seisakusho, Tokyo, Japan) and were average about 30 ± 1 μm.

2.4. Gas permeation experiments

The pure gas permeability was measured by variable feed pressure and the constant volume permeation method. All the membrane samples were tested at room temperature (~25

°C) and the test pressure in the range of 2-10 bar. The rate of pressure increase (*dp/dt*) at the permeate side at steady state was measured by an absolute pressure transmitter (type 691, pressure range of 0-0.1 bar, accuracy of ± 0.3% full scale, Huba Control, Würenlos, Switzerland) and used to calculate the permeability using the following equation:

$$P = \frac{273.15 \times 10^{10} Vl}{AT(p_0 \times 76)}\left(\frac{dp}{dt}\right) \quad (1)$$

where P is the gas permeability in Barrer (1 Barrer = 1 cm^3 (STP) cm/cm^2 cmHg s), V is the dead-volume of the downstream chamber (cm^3), l is the membrane thickness (cm), p_0 is the feed pressure (atm), and *dp/dt* is the steady rate of pressure increase in the downstream side (atm/s), A is the effective membrane area (cm^2) with the value of 15.9 cm^2, and T is the absolute temperature (K). It should be noted that to ensure the accuracy of the data acquisitions, each measurement replicated on the three different membrane samples with the same composition and the reported value is the arithmetic mean of the three samples.

In addition, the ideal selectivity of two pure components was calculated by dividing the respected permeabilities in the same conditions.

$$\alpha_{A/B} = \frac{P_A}{P_B} \quad (2)$$

where P_A and P_B are the permeability of pure gases A and B, respectively.

2.5. Characterizations

Dynamics light scattering (DLS) analysis was done on the solid NaY zeolite powder as well as the silane-modified one (NaY-sm) to determine the particle-size distribution (PSD). DLS analysis was performed with a Scatteroscope-I advanced DLS type nano-micro particle size analyzer (Qudix Inc., Seoul, Korea) on the zeolite powders suspended in water (22 °C) to determine the particle sizes and distributions, based on the intensity of light scattered. The

total exposure time taken for DLS analysis was 8 s with the exposure time length of 0.246 s. The experiment produced an average count rate (scattering intensity) of 217 kcps, in kilocounts per second, where:

$$\text{Average count rate} \propto (\text{diameter of particles})^6 \times (\text{number of particles})$$

In order to characterize the textural properties of the particles the Brunauer–Emmett–Teller (BET) surface area and volume of micro pores were determined by N_2 adsorption–desorption isotherms at liquid nitrogen (76 K) using TriStar II 3020 V1.03 analyzer (Micromeritics Instrument Co., Norcross, GA) after degassing the samples at 150 °C for at least 4 h under vacuum (< 10^{-3} Pa). The linear part of the (BET) equation (p/p_0= 0.05–0.3) was used to calculate the BET surface area. The t-plot method was applied to determine the micro pore volume of the particles.

Fourier transform infrared-attenuated total reflectance (FTIR-ATR) spectroscopy was done on the zeolites and membrane samples using a Perkin-Elmer Spectrum, Frontier model, Version 10.03.06 (Perkin-Elmer Instruments, Norwalk, USA) in the range of 600-4000 cm^{-1}. In the case of liquid silane coupling agent, the FTIR spectrum was done in the transition mode. The spectrum of each specimen was taken at an incidence angle of 458 with 32 scans at a wave number resolution of 4 cm^{-1}.

The X-ray diffraction (XRD) patterns of the membranes were analyzed on an X'Pert MPD wide-angle X-ray diffractometer from Philips, The Netherlands. The measurements were carried out at room temperature using monochoromatic radiation of α-rays emitted by Cu at a wave-length of 1.54 Å, accelerating voltage of 40 kV, and tube current of 40 mA. To identify the crystal structure, the scan range - the angle (2θ) of diffraction - was varied from 3 to 70° with a step increment of 0.02° s^{-1}.

The morphological observation of the zeolites and membrane samples were carried out by scanning electron microscopy (SEM). After sputter-coating with gold by a BAL-TEC SCD

005 sputter coater (BAL-TEC AG, Balzers, Liechtenstein), the samples were tested by a SEM (KYKY-EM3200, KYKY Technology Development Ltd., Beijing, China). In the case of cross section observations of membranes, the samples were fractured in liquid nitrogen.

Thermal analyses of the membranes were carried out using TG/DTA. The TG/DTA measurements were carried out by using a Bahr (Wetzlar, Germany) STA-503 instrument. TG/DTA runs were recorded at a scan rate of 10° min^{-1} up to 600 °C. The sample compartment was flushed with dried, ultra high pure argon at all times.

3. Results and discussion

3.1. Characterizations

3.1.1. DLS

The results of DLS analyses for pure and silylated zeolites were summarized in Table 1. As can be expected, the particle size distributions are shifted towards higher values with the modification reaction. The average particle diameter of silylated zeolites undergoes from 1.22 to 1.74 μm, a ~43 % increase. The increase in particle sizes is very far from the previously mentioned distance of around 5–9 Å which was due to the presence of APDEMS between polymer chains and the zeolite surface. This can be due to a crosslinking reaction occurring simultaneously with the silylation. The silanol groups of APDEMS can react with each other by crosslinking to form Si−O−Si linkages. Therefore, a three-dimensional network is formed around a zeolite particle.[17]

3.1.2. BET

A summary of the BET results for pure and silylated zeolites are listed in Table 2. As can be seen, both the (BET and micropore) surface areas and (micro- and total pore) volumes show a decrease about half of their initial values with the silylation reaction. This is while the

particle external surface area increases about 65% and the average pore diameter does not change significantly. These observations can be initially emphasized firstly on the blockage or narrowing a significant portion of zeolite openings by the silane coupling agents in the silylation reaction.[32] Secondly, it suggests the success in a proper surface modification reaction which results in an increased external surface area and overall volume (or size) of zeolite particles, well consistent with the DLS results.

3.1.3. FTIR-ATR

FTIR-ATR spectra of (a) silane coupling agent, (b) NaY zeolite, (c) silylated zeolite (NaY-sm), (d) neat CA and the related MMMs containing 20 wt.% NaY (e) and NaY-sm (f) zeolites are shown in Figure 2. The FTIR spectrum of liquid APDEMS as the silane coupling agent is also presented in the spectrum (a) in Figure 2. The peak at 3354 cm^{-1} corresponds to −OH stretching vibrations of the hydroxyl group. This is also caused by overlapping the $–NH_2$ stretching of primary amine in the spectra (3500−3300 cm^{-1}), which appear approximately at the same frequency of −OH stretching. In this case, the corresponding –NH bending vibration is located at 1575 cm^{-1}. The absorption peaks at 2973, 2926, and 2879 cm^{-1} are corresponded respectively to $–CH_3$, $–CH_2$ and –CH asymmetric stretching vibrations. The corresponding bending vibrations of $–CH_3$ and $–CH_2$ are located at 1390 and 1482 cm^{-1}, respectively. The characteristic alkoxy or ether absorption bands of the sample appeared at 1258 cm^{-1} for C−C−O stretching and two absorption bands around 950 to 750 cm^{-1} (C−O stretching), in accordance with Lou *et al.*[33]. Strong absorptions around 1100−1075 cm^{-1} together with a weak absorption at ~1165 cm^{-1} are corresponded to $Si–O–C_2H_5$ vibrations. Moreover, the absorption peaks at 1297 and 1258 cm^{-1} are respectively attributed to $Si–CH_3$ and $Si–CH_2–$ stretching vibrations, where the latter appeared at the same frequency of alkoxy C−C−O stretching.[34] In the FTIR spectrum (b) in Figure 2, for the NaY zeolite, a

characteristic broad peak at 3650−3200 cm^{-1} is corresponded to Si−OH stretching. The related Si−OH bending vibration (~900−850 cm^{-1}) appeared together with the Si−O−Si vibration (1100−1000 cm^{-1}) as another characteristic peak for the zeolite at 1100−850 cm^{-1}. In the case of silylated zeolite, the FTIR spectrum (c) in Figure 2, the absorption peaks at 1307 and 1263 cm^{-1} are those strengthened by Si−CH_3 and Si−CH_2− stretching vibrations of the grafted groups. Moreover, the absorption peaks at 2966 and 2920 cm^{-1} are those of strengthened by −CH_3 and −CH_2 stretching vibrations of the grafted groups.[35] On the other hand, a typical absorption of the –NH_2 stretching of primary amine (3500−3300 cm^{-1}) can weaken the −OH stretching vibrations of the zeolite hydroxyl groups. Thus, the FTIR results demonstrate that the surface of NaY zeolite has been successfully modified by silylation reaction without altering the zeolite structure. In the FTIR-ATR spectrum of the neat CA membrane, spectrum (d) in Figure 2, a broad band at 3484 cm^{-1} represents OH^- stretching vibrations of the hydroxyl group in the CA membrane.[36] In addition, a band at 1637 cm^{-1} is attributed to the interlayer stretching and bending vibration modes of molecular water. The characteristic peaks of CA at 1738 (C=O stretching), 1368 (CH_3 symmetric deformation), 1220 (acetate C−C−O stretching), and 1035 (C−O stretching) cm^{-1} are clearly observed which are generally in accordance with Yang[37] and Benosmane *et al*.[38]. Furthermore, absorptions at 2942 and 1432 cm^{-1} are respectively attributed to CH_3 asymmetric stretching and CH_3 asymmetric deformation. The characteristic peaks of saccharide structure of CA are observed at around 1161 (stretching of the C−O− bridge), 1122 and 1035 (skeletal vibration involving the C−O stretching) cm^{-1}. The absorption band at 901 cm^{-1} is attributed to the β−linked glucan structure.[39] In addition, a small absorption peak is observed at ~2119 cm^{-1} for a high temperature dried CA which is assigned to a heat-dissociated or weakly bond −C≡C−, a characteristic absorption of the acetylene. This can be observed as an enough thermal energy required for disassociation of intra- and/or inter-molecular hydrogen bonding is adsorbed

which leads to formation of a methylenic proton ($OCH_2-C\equiv C-$). Therefore, it is suggested that a rearrangement reaction had taken place to yield a new fragment.[40] In the FTIR-ATR spectra of NaY and NaY-sm filled membranes, respectively in spectra (e) and (f) in Figure 2, the peak intensities of CA are generally decreased by incorporating both the pure and silylated zeolites into the polymer matrix, with a severe reduction for NaY-sm compared with NaY. However, the intensities of multiple characteristic peak of neat CA in the range of 1200 to 1000 cm^{-1}, which corresponded to C−O stretching vibrations, show less reduction upon introducing the zeolite in the membrane. This is caused by overlapping the Si−O stretching of zeolites in the spectra, which appear approximately at the same frequency of C−O stretching.[41, 42] This is repeated almost in the range of 800−600 cm^{-1} which may be corresponded to Al−O stretching vibrations.[39]

3.1.4. XRD

XRD patterns of NaY zeolites before (a) and after silane modification (b) are presented in Figure 3. In addition, the XRD patterns of the pure CA membrane (c) and mixed matrix membranes containing 20 wt.% NaY (d) and NaY-sm (e) are also depicted. NaY zeolite exhibits all the characteristic peaks corresponding to the Kariduraganavar *et al*.[43] and Ma *et al*.[44], indicating that the sample is pure Faujasite (FAU) phase. The crystalline structure of NaY zeolite may be slightly disrupted during the surface modification by APDEMS, resulting in a slight decrease in the peak intensities, and in turn, the crystallinity of NaY-sm zeolite in comparison to the pure NaY. It is of interest to note that this decrease in the XRD peaks of NaY crystals may also be explained by considerable changes caused by silylation reaction in the surface, opening and/or channels of the zeolite, where the APDMS does not exist in the crystalline state. CA has two broad crystalline peaks at 12° and 22°, in accordance with Achoundong *et al*.[45] and Ma *et al*.[42]. After incorporating the NaY or NaY-sm zeolites into

CA, the membrane patterns show the characteristic peaks of both the zeolites and CA. However, a slight decrease in the intensity of CA peaks suggests that the CA loses a number of its crystallinity in the presence of zeolites.

3.1.5. SEM

Figure 4a, b shows the SEM images of NaY and NaY-sm zeolite powders. A three-dimensional crystalline structure is observed for the NaY zeolites with the particle sizes ranging mainly from about 1-1.5 μm (Figure 4a). Another noticeable observation is the existence of some small aggregates (~2-4 μm) that consist of only a few adjoined particles. The issue enhances for silylated zeolites with more tendency to form larger aggregates due to new adhesive forces between amine functional groups of the surface modified zeolites. This causes some new crystals to form, having hexagonal plates with small octahedra growing from the surface which consequently results in forming those shaped in Figure 4b as twined particles[46]. These are in a less degree of crystallinity that is previously demonstrated by the XRD spectra. Generally, the SEM results for zeolite sizes are consistent with the previous results of DLS and BET analyses.

SEM images of cross section and surface of the neat CA membrane (Figures 5a and b) show a dense and uniform structure with no defect all over the membrane areas. Moreover, a rather rough cross sectional area is shown while a very smoother surface is found for the membrane. As can be seen for unmodified NaY zeolite loaded membranes (Figures 5c to e), more of the zeolite particles are properly distributed in the polymer matrix. However, there are a few agglomerates which are intensified at higher zeolite contents and coincided with the improper particle aggregates.[36] These are inaccessible points for the gas molecules to pass through and can act as dead zones in the membrane matrix. The aminosilane modified zeolites provide an improved filler-polymer interfacial adhesion due to the acid-base ionic

interactions of NH groups on the surface of the modified zeolite with the carbonyl (−CO) and oxycarbonyl (−COO) groups of CA in order to form hydrogen bonds. A similar hypothesis was previously suggested by Nik *et al*.[47] for APMDES modified zeolites with polyimide. As can be seen in the magnified cross section images of NaY-sm loaded CA membranes (Figures 5g to i), the surface modified zeolites significantly improve the particle distribution and can also lead to a shift of undesirable cracks towards a lesser extent. Moreover, the cracks are properly vanished at higher NaY-sm loadings. Finally, comparing the surface images of neat CA (Figure 5b) with those containing NaY and NaY-sm (Figures 5f and j) shows that the membrane surfaces roughened by incorporation of zeolites, more evident for NaY rather than NaY-sm filled membranes. This can also be another sign of reduction in the number or size of the agglomerates by using the modified zeolites.

3.1.6. TG/DTA

Figure 6 shows TGA spectra of the neat CA membrane and the related mixed matrix membranes containing 5, 20 and 25 wt.% of NaY and NaY-sm zeolites. A three-step degradation can be observed for all the membrane samples. An initial weight loss of ~5% before 350 °C is observed for all the membrane samples due to elimination of the physisorbed water molecules or remaining solvents in the samples. Afterwards, the mass loss curves undergo a major decomposition step which takes place in temperatures of 350-400 °C, well consistent with the results obtained by Ma *et al*.[42] for 0.3-0.5 μm sized HZSM5-filled CA membranes. It is worthy to note that the decomposition of grafted silane takes place from 300 to 450 °C,[48] and hence, its major decomposition overlaps with the observed second step. The final decomposition step starts at ~400 °C and reaches a horizontal asymptote next to 580 °C.

Although the origin of the poor/perfect compatibility between the interphases is complicated, silane modified zeolite surfaces can improve the interfacial strength between two interphases, the dispersed zeolite and polymer matrix.[26] This results in an almost better thermal stability of the NaY-sm loaded membrane samples in comparison with the NaY loaded ones. This can be observed in the data that was obtained by DTA analysis and summarized in Table 3. A significant decline in thermal stability of the membranes can also be seen with 5 wt.% NaY (T_g = 174 °C, main step decomposition starts at 305 °C) or NaY-sm (T_g = 174 °C, main step decomposition starts at 307 °C) compared to the neat CA membrane (T_g = 191 °C, main step decomposition starts at 341 °C). A substantial decrease (~14%) in T_gs of a MMM based on the glassy (polyimide) polymers at the lower loadings of larger micron-sized zeolite 13X, against an increase in T_gs by incorporating the smaller nano-sized 4A types, was also reported by Boroglu and Gurkaynak.[49] Generally, in the CA/NaY membranes can observe a more stability for the membrane containing 20 wt.% NaY. However, the amino silane modified zeolites cause a slight increase in the stability of CA/NaY-sm membrane samples from 5 to 25 wt.%.

3.2. Gas permeation

Concerning gas separation performance of the aminosilane modified zeolite-filled cellulose acetate membranes, the CO_2 and N_2 permeation measurements were conducted at different modified zeolite loadings (0-25 wt.%) as well as multiple pressures (2-10 bar). Moreover, the NaY-sm contained MMMs are compared with those filled with pure NaY zeolites.

Figure 7 shows the effect of NaY-sm particle loadings on the (a) CO_2 permeability and (b) CO_2/N_2 selectivity of the membranes. The reaction mechanism of CO_2 with the amines immobilized on a solid carrier has been extensively analyzed.[50-53] Generally, it is very

complicated as the additional occurrence of physisorption on the surface and the open pores of the solid supports. However, a typical reaction pathway that is frequently presented for the immobilized primary amines is as follows:[51]

$$CO_2 + RNH_2 + RNH_2 \rightleftharpoons RNHCO_2^- + RNH_3^+ \quad (3)$$

$$CO_2 + RNH_2 + H_2O \rightleftharpoons HCO_3^- + RNH_3^+ \overset{pH}{\rightleftharpoons} RNH_3^+ + CO_3^{2-} \quad (4)$$

which the Eqs. (3) and (4) are associated to the dry and wet CO_2 chemisorption processes, respectively. The values of −50 to −118 kJ/mol CO_2 were reported for enthalpy change of reaction for dry CO_2 chemisorption. The value of −56 kJ/mol CO_2 and additionally −47 to −53 kJ/mol for H_2O were also reported for wet CO_2 chemisorption. The formation of the carbamate ion ($RNHCO_2^-$) at dry sorption and bicarbonate (HCO_3^-) and carbonate (CO_3^{2-}) ions at wet sorption is observed.[53] It is well established that not only the formation of carbamate (Eq. 3, an amine/CO_2 feed ratio of 2) is much faster than the formation of bicarbonate as the limiting stoichiometry for chemisorption of CO_2 (Eq. 4, an amine/CO_2 feed ratio of 1), but also for practical purposes the formation of bicarbonate is only observed when a long contact time is permitted. In addition, humid CO_2 adsorption is significantly dependent on CO_2 pressure, relative humidity of the feed and the proper surface and/or capillary water condensation in the solid supports, and the accessibility of active sites.[51] It is also stated that exceeding a determined water content in the CO_2 streams leads to a decrease in the CO_2 adsorption capacity due to the competitive adsorption between CO_2 and H_2O at the same adsorption sites. Although modification of the zeolite surface with the aminosilane coupling agent results in a significant increase towards a high hydrophobic material compared to the pristine zeolite, it still contains some −OH groups (see FTIR spectra, Figure 2) which make it slightly hydrophilic. Thus, in addition to dry CO_2 adsorption by

aminosilane-functionalized zeolite, further CO_2 can be adsorbed in the presence of some amount of moisture. This can also lead to regenerating amine molecules as:[52]

$$RNHCO_2^- + H_2O \rightleftharpoons RNH_2 + HCO_3^- \quad (5)$$

The increase in CO_2 permeability with the increase in the amounts of NaY-sm zeolites (Figure 7a) can now be explained according to the above mentioned mechanisms. The more the NaY-sm loadings in the CA matrix, the further the CO_2 molecules can be adsorbed. This results in a facilitated transport of CO_2 molecules via the NaY-sm zeolites in addition to that occurred by solution and diffusion of CO_2 through the CA matrix. Therefore, a considerable increase in CO_2 permeabilities, for example ~40 % increase from 2.63 to 3.67 Barrer (at 2 bar), can be observed by only 5 wt.% of NaY-sm loading into the CA. Afterwards, a milder growth is observed in CO_2 permeabilities with the increment in NaY-sm contents up to 25 wt.%. This may be due to the effect of agglomerates that are further formed in the high NaY-sm filled membrane samples and cause a difficulty to gas transport through the membranes. In case of CO_2/N_2 selectivity, Figure 7b, a slow decrease is observed at all pressures up to 15 wt.% NaY loading, and then it approaches a maximum at 20 wt.% and finally it experiences a severe decline at 25 wt.%. This maximum at high loading of 20 wt.% NaY-sm can be due to the greater formation of carbamate ions at the particle surfaces according to Eq. 3 and their lower disassociation rates, specially at higher CO_2 concentrations (or the pressures higher than 4 bar). This can result in a considerable accumulation of adsorbed CO_2 molecules which are trapped in the polymer/particle interfaces and consequently lead to bottlenecking the pathways of N_2 molecules across the membrane (Figure 8). However, more particle loading from 20 to 25 wt.% in Figure 7b results in a significant decline in CO_2/N_2 selectivity of the membrane due to reaching a "percolation threshold" (the critical volume fraction of the filler). This means an interconnection of particles and/or agglomerates to each other to form

non-selective pathways across the membranes (see discussions on SEM observations, section 3.1.5).

Figure 9 presents the effect of feed pressure, from 2 to 10 bar, on the CO_2 permeability and CO_2/N_2 selectivity of the CA/NaY-sm membranes. As can be seen in Figure 9a, CO_2 permeabilities of all the membrane samples decrease as the pressure increases. This is a common behavior of glassy polymers and also their MMMs below the plasticization pressure.[54-57] An increase in feed pressure forces the polymer chains to form a closer packing density and thus decreasing the gas permeability. As there is not enough considerable difference between effective molecular diameters of CO_2 and N_2 (the most widely used scales of these gases for diffusion through the polymeric membranes is the so-called kinetic diameter which is respectively 3.3 and 3.64 Å for CO_2 and N_2)[58], the same behavior can occur for selectivities,[59-61] Figure 9b. A severe decline in selectivity of the CA/NaY-sm 25 wt.% membrane sample with the increase in pressure is due to reaching a percolation limit of the solid particles.

Figure 10 presents a comparison between the performance of CA/NaY mixed matrix membranes[36] and those filled with NaY-sm. At lower particle loadings (≤ 15 wt.%), it is observed an increase in CO_2 permeability of the NaY-sm loaded MMMs compared to those filled with NaY zeolites. According to a review conducted by Basu *et al*.[31] on the strategies to enhance filler/polymer compatibility, the introduction of trimethylsilyl-glucose (TMSG) into a glassy cellulose ester structure leads to a significant increase in gas permeability due to the action as a plasticizer, thereby increasing the chain mobility. On the other hand, Calabrese *et al*.[17] showed an occurrence of a crosslinking reaction between the silanol groups of coupling agents to form intermolecular Si−O−Si linkages (see discussions on DLS results, section 3.1.1). It can be concluded from these two studies that the crosslinked network formed by APDEMS molecules on the zeolite surfaces may act as plasticized regions, owing to the

motions of CH_3 and NH_2 side groups. The amine functional groups of organosilanes provide a potential for various polar and hydrophobic interactions with CO_2 molecules.[25] On the other hand, by further increasing the amounts of NaY-sm (≥ 20 wt.%) into the CA matrix and the subsequent increase in the amounts of pores blocked by the silane molecules, pore blockage becomes more prominent to a decrease in CO_2 permeability of NaY-sm as compared to more facilitation of CO_2 transport by open pores of the NaY zeolites. Therefore, non-interacting or just diffusive N_2 molecules suffer more from the issue.[62] This can result in a higher selectivity of NaY-sm loaded MMMs in all cases.

4. Conclusion

3-aminopropyl(diethoxy)methylsilane (APDEMS) was used for silylation of NaY zeolite surface in order to investigate the effect of surface modified zeolite (NaY-sm) in cellulose acetate (CA) gas separation membranes. The results of chemical/structural analyses showed an achievement in a proper silane modification reaction and also a morphological improvement of the prepared mixed matrix membranes (CA/NaY-sm) in comparison with the CA/NaY membranes. In most cases, better gas permeation results were obtained using the NaY-sm instead of NaY in the membranes. An optimum permselectivity behavior obtained by a 20 wt.% NaY-sm loading into the CA matrix whereas at pressure of 2 bar, CO_2 permeability increased from 2.63 to 4.63 Barrer (up to 76 %) for CA/NaY-sm 20 wt.% membrane as compared to the neat CA membrane. This coincided with no considerable decline in the CO_2/N_2 selectivity. Even a slight increase of an average 6.34 % was also observed in the selectivity of the membranes at higher pressures (≥ 4 bar).

Acknowledgements

We thank Abtin Ebadi Amooghin (Department of Chemical Engineering, Tarbiat Modares University, Tehran, Iran) for his kind assistance.

References

1. S. Sanaeepur, H. Sanaeepur, A. Kargari and M. H. Habibi, *Int. J. Sustain. Energ.*, 2014, **33**, 203-212.

2. A. Kargari and M. Takht Ravanchi, in *Greenhouse gases- capturing, utilization and reduction*, ed. G. Liu, InTech, Rijeka, Croatia, 2012, ch. 1, pp. 3-30.

3. M. Takht Ravanchi, T. Kaghazchi and A. Kargari, *Desalination*, 2009, **235**, 199–244.

4. Y. Li, G. He, S. Wang, S. Yu, F. Pan, H. Wu and Z. Jiang, *J. Mater. Chem. A*, 2013, **1**, 10058-10077.

5. C. Liu, S. Kulpathipanja, A. M. W. Hillock, S. Husain and W. J. Koros, in *Advanced membrane technology and applications*, eds. N. N. Li, A. G. Fane, W. S. Winston Ho and T. Matsuura, John Wiley & Sons Ltd., Hoboken, New Jersey, 2008, pp. 789-819.

6. G. Dong, H. Li and V. Chen, *J. Mater. Chem. A*, 2013, **1**, 4610-4630.

7. T.-H. Bae, J. Liu, J. S. Lee, W. J. Koros, C. W. Jones and S. Nair, *J. Am. Chem. Soc.*, 2009, **131**, 14662–14663.

8. M. E. Lydon, K. A. Unocic, T.-H. Bae, C. W. Jones and S. Nair, *J. Phys. Chem. C*, 2012, **116**, 9636-9645.

9. S. Shu, S. Husain and W. J. Koros, *J. Phys. Chem. C*, 2007, **111**, 652-657.

10. W.-G. Kim, X. Zhang, J. S. Lee, M. Tsapatsis and S. Nair, *ASC nano*, 2012, **6**, 9978-9988.

11. M. Rezakazemi, A. Ebadi Amooghin, M. M. Montazer-Rahmati, A. F. Ismail and T. Matsuura, *Prog. Polym. Sci.*, 2014, **39**, 817-861.

12. C. I. Chaidou, G. Pantoleontos, D. E. Koutsonikolas, S. P. Kaldis and G. P. Sakellaropoulos, *Sep. Sci. Technol.*, 2012, **47**, 950-962.

13. D. Şen, H. Kalıpçılar and L. Yilmaz, *J. Membr. Sci.*, 2007, **303**, 194-203.

14. C. V. Funk and D. R. Lloyd, *J. Membr. Sci.*, 2008, **313**, 224–231.

15. J.-T. Chen, C.-C. Shih, Y.-J. Fu, S.-H. Huang, C.-C. Hu, K.-R. Lee and J.-Y. Lai, *Ind. Eng. Chem. Res.*, 2014, **53**, 2781-2789.

16. M. U. M. Junaidi, C. P. Khoo, C. P. Leo and A. L. Ahmad, *Micropor. Mesopor. Mat.*, 2014, **192**, 52-59.

17. L. Calabrese, L. Bonaccorsi and E. Proverbio, *J. Coat. Technol. Res.*, 2012, **9**, 597-607.

18. H. Zhou, Y. Su, X. Chen, S. Yi and Y. Wan, *Sep. Purif. Technol.*, 2010, **75**, 286–294.

19. Y. Zhang, J. Sunarso, S. Liu and R. Wang, *Int. J. Greenh. Gas Cont.*, 2013, **12**, 84-107.

20. T. T. Moore and W. J. Koros, *Ind. Eng. Chem. Res.*, 2008, **47**, 591-598.

21. B.-Z. Zhan, M. A. White and M. Lumsden, *Langmuir*, 2003, **19**, 4205-4210.

22. Z. n. Bacsik, N. Ahlsten, A. Ziadi, G. Zhao, A. E. Garcia-Bennett, B. n. Martín-Matute and N. Hedin, *Langmuir*, 2011, **27**, 11118-11128.

23. C.-H. Cheng, T.-H. Bae, B. A. McCool, R. R. Chance, S. Nair and C. W. Jones, *J. Phys. Chem. C*, 2008, **112**, 3543-3551.

24. D. M. Pacheco, J. R. Johnson and W. J. Koros, *Ind. Eng. Chem. Res.*, 2012, **51**, 503-514.

25. M. H. Kassaee, D. S. Sholl and S. Nair, *J. Phys. Chem. C*, 2011, **115**, 19640–19646.

26. X. Y. Qu, H. Dong, Z. J. Zhou, L. Zhang and H. L. Chen, *Ind. Eng. Chem. Res.*, 2010, **49**, 7504–7514.

27. M. A. Aroon, A. F. Ismail, T. Matsuura and M. M. Montazer-Rahmati, *Sep. Sci. Technol.*, 2010, **75**, 229–242.

28. T.-S. Chung, L. Y. Jiang, Y. Li and S. Kulprathipanja, *prog. Polym. Sci.*, 2007, **32**, 483–507.

29. G. Clarizia, C. Algieri, A. Regina and E. Drioli, *Micropor. Mesopor. Mat.*, 2008, **115**, 67–74.

30. Y. Li, H.-M. Guan, T.-S. Chung and S. Kulprathipanja, *J. Membr. Sci.*, 2006, **275**, 17-28.

31. S. Basu, A. L. Khan, A. Cano-Odena, C. Liu and I. F. J. Vankelecom, *Chem. Soc. Rev.*, 2010, **39**, 750-768.

32. H. Liu, Y. Li, W. Shen, X. Bao and Y. Xu, *Catal. Today*, 2004, **93-95**, 65-73.

33. Y. Lou, G. Liu, S. Liu, J. Shen and W. Jin, *Appl. Surf. Sci.*, 2014, **307**, 631-637.

34. D. L. Pavia, G. M. Lampman, G. S. Kriz and J. R. Vyvyan, *Introduction to spectroscopy*, Brooks/Cole, Belmont, CA, 4th edn., 2009.

35. P. Wei, X. Qu, H. Dong, L. Zhang, H. Chen and C. Gao, *J. Appl. Polym. Sci.*, 2013, **128**, 3390-3397.

36. H. Sanaeepur, B. Nasernejad and A. Kargari, *Greenhouse Gas. Sci. Technol.*, accepted manuscript, Oct. 27, 2014.

37. Y. Yang, in *Polymer data handbook*, ed. J. E. Mark, Oxford University Press, New York, 1999, pp. 49-56.

38. N. Benosmane, B. Guedioura, S. M. Hamdi, M. Hamdi and B. Boutemeur, *Mat. Sci. Eng. C*, 2010, **30**, 860-867.

39. H. Dogan and N. D. Hilmioglu, *Vacuum*, 2010, **84**, 1123-1132.

40. C. Badarau and Z. Y. Wang, *Macromolecules*, 2004, **37**, 147-153.

41. A. A. Kittur, S. S. Kulkarni, M. I. Aralaguppi and M. Y. Kariduraganavar, *J. Membr. Sci.*, 2005, **247**, 75-86.

42. X. Ma, C. Hu, R. Guo, X. Fang, H. Wu and Z. Jiang, *Sep. Purif. Technol.*, 2008, **59**, 34-42.

43. M. Y. Kariduraganavar, A. A. Kittur, S. S. Kulkarni and K. Ramesh, *J. Membr. Sci.*, 2004, **238**, 165-175.

44. N. Ma, J. Wei, R. Liao and C. Y. Tang, *J. Membr. Sci.*, 2012, 405-406, 149-157.

45. C. S. K. Achoundong, N. Bhuwania, S. K. Burgess, O. Karvan, J. R. Johnson and W. J. Koros, *Macromolecules*, 2013, **46**, 5584-5594.

46. O. G. Nik, B. Nohair and S. Kaliaguine, *Micropor. Mesopor. Mat.*, 2011, **143**, 221-229.

47. O. G. Nik, X. Y. Chen and S. Kaliaguine, *J. Membr. Sci.*, 2011, **379**, 468-478.

48. S. Khemakhem and R. B. Amar, *Colloid. Surface. A: Physicochem. Eng. Aspects*, 2011, **387**, 79–85.

49. M. S. Boroglu and M. A. Gurkaynak, *Polym. Bull.*, 2011, **66**, 463-478.

50. X. Zhang, S. Schubert, M. Gruenewald and D. W. Agar, *Chem. Eng. J.*, 2005, **107**, 97-102.

51. R. Serna-Guerrero, E. Da'na and A. Sayari, *Ind. Eng. Chem. Res.*, 2008, **47**, 9406-9412.

52. F. Su, C. Lu, S.-C. Kuo and W. Zeng, *Energ. Fuel.*, 2010, **24**, 1441-1448.

53. C. Gebald, J. A. Wurzbacher, P. Tingaut, T. Zimmermann and A. Steinfeld, *Environ. Sci. Technol.*, 2011, **45**, 9101–9108.

54. A. Ebadi Amooghin, H. Sanaeepur, A. Moghadassi, A. Kargari, D. Ghanbari and Z. Sheikhi Mehrabadi, *Sep. Sci. Technol.*, 2010, **45**, 1385-1394.

55. A. Ebadi Amooghin, H. Sanaeepur, A. Kargari and A. Moghadassi, *Sep. Purif. Technol.*, 2011, **82**, 102-113.

56. H. Sanaeepur, A. Ebadi Amooghin, A. Moghadassi, A. Kargari, S. Moradi and D. Ghanbari, *Polym. Adv. Technol.*, 2012, **23**, 1207-1218.

57. O. Hosseinkhani, A. Kargari and H. Sanaeepur, *J. Membr. Sci.*, 2014, **469**, 151-161.

58. S. Matteucci, Y. Yampolskii, B. D. Freeman and I. Pinnau, in *Materials science of membranes for gas and vapor separation*, eds. Y. Yampolskii, I. Pinnau and B. D. Freeman, John Wiley & Sons Ltd., West Sussex, United Kingdom, 2006, pp. 1-47.

59. H. Sanaeepur, A. Ebadi Amooghin, A. Moghadassi and A. Kargari, *Sep. Purif. Technol.*, 2011, **80**, 499-508.

60. S. Bandehali, A. Kargari, A. Moghadassi, H. Saneepur and D. Ghanbari, *Asia-Pac. J. Chem. Eng.*, 2014, **9**, 638–644.

61. M. Omidkhah, M. Zamani Pedram and A. Ebadi amooghin, *J. Membra. Sci. Technol.*, 2013, **3**, 119.

62. J.-M. Duval, A. J. B. Kemperman, B. Folkers, M. H. V. Mulder, G. Desgrandchamps and C. A. Smolders, *J. Appl. Polym. Sci.*, 1994, **54**, 409-418.

Table captions:

Table 1. DLS results of NaY and NaY-sm zeolite powders suspended in water (22 °C).

Table 2. BET results of NaY and NaY-sm zeolite powders.

Table 3. Summary of DTA data of CA and its MMMs containing NaY and NaY-sm zeolites.

Table 1. DLS results of NaY and NaY-sm zeolite powders suspended in water (22 °C).

Distribution (%, intensity)		d(0)	d(5)	d(10)	d(25)	d(50)	d(75)	d(90)	d(95)	d(100)	Averaged
Particle size diameter (μm)	**NaY**	0.308	0.672	0.762	0.948	1.22	1.56	1.95	2.20	4.81	**1.22**
	NaY-sm	0.054	0.933	1.07	1.36	1.74	2.20	2.79	3.16	6.90	**1.74**

Table 2. BET results of NaY and NaY-sm zeolite powders.

Sample	BET surface area (m^2/g)	micro pore volume (cm^3/g)	total pore volume (cm^3/g)[a]	micro pore surface area (m^2/g)[b]	external surface area (m^2/g)[c]	average pore diameter (nm)[d]
NaY	619	0.285	0.297	596	16.6	1.92
NaY-sm	313	0.137	0.155	285	27.4	1.97

[a] single point desorption total pore volume of pores less than 84.11 nm width at $p/p_0 = 0.98$

[b,c] calculated by the t-plot method

[d] desorption average pore width (4V/A by BET)

Table 3. Summary of DTA data of CA and its MMMs containing NaY and NaY-sm zeolites.

Membrane	Transition temperature (°C)					
	onset 1	max 1	onset 2	max 2	onset 3	max 3
CA	44	191	341	374	396	440
CA/NaY 5 wt.%	39	174	305	359	390	511
CA/NaY 20 wt.%	33	210	352	377	395	402
CA/NaY 25 wt.%	53	181	324	354	387	408
CA/NaY-sm 5 wt.%	76	174	307	367	387	415
CA/NaY-sm 20 wt.%	84	178	330	373	393	515
CA/NaY-sm 25 wt.%	102	181	331	359	388	407

Figure captions:

Figure 1. A schematic of chemical modification of the zeolite surface.

Figure 2. FTIR-ATR spectra of (a) the silane coupling agent (APDEMS), (b) NaY zeolite, (c) silylated NaY zeolite (NaY-sm), (d) neat CA membrane, (e) CA/NaY (20 wt.%), and (f) CA/NaY-sm (20 wt.%) mixed matrix membranes.

Figure 3. XRD patterns of (a) NaY zeolite, (b) silylated NaY zeolite (NaY-sm), (c) neat CA membrane, (d) CA/NaY (20 wt.%), and (e) CA/NaY-sm (20 wt.%) mixed matrix membranes.

Figure 4. SEM images of (a) NaY and (b) NaY-sm powders.

Figure 5. SEM images of the prepared membranes: (a) CA (cross), (b) CA (surface), (c) CA/NaY 5 wt.% (cross), (d) CA/NaY 20 wt.% (cross), (e) CA/NaY 25 wt.% (cross), (f) CA/NaY 20 wt.% (surface), (g) CA/NaY-sm 5 wt.% (cross), (h) CA/NaY-sm 20 wt.% (cross), (i) CA/NaY-sm 25 wt.% (cross), and (j) CA/NaY-sm 20 wt.% (surface).

Figure 6. TGA spectra of the neat CA membrane and the related mixed matrix membranes containing NaY and NaY-sm zeolites.

Figure 7. The effect of NaY-sm particle loadings on (a) CO_2 permeability and (b) CO_2/N_2 selectivity; the lines are only a guide to the eye.

Figure 8. A schematic representation for CO_2/N_2 selectivity improvement via the facilitated CO_2 transport in the CA/NaY-sm membranes; the most widely used kinetic diameter was chosen for the effective molecular diameters of the penetrant gases which are respectively 3.3 and 3.64 Å for CO_2 and N_2 molecules.

Figure 9. The effect of feed pressure on (a) CO_2 permeability and (b) CO_2/N_2 selectivity; solid lines are used only for connecting the data; the lines are only a guide to the eye.

Figure 10. Comparing the performance of NaY and NaY-sm zeolites in the MMMs at 4 bar.

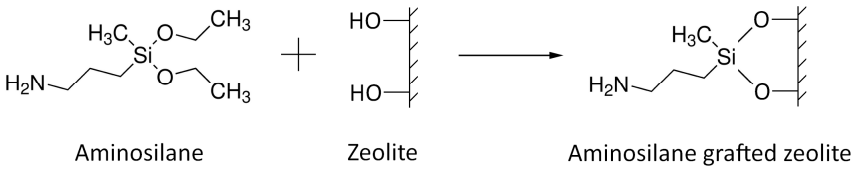

Figure 1. A schematic of chemical modification of the zeolite surface.

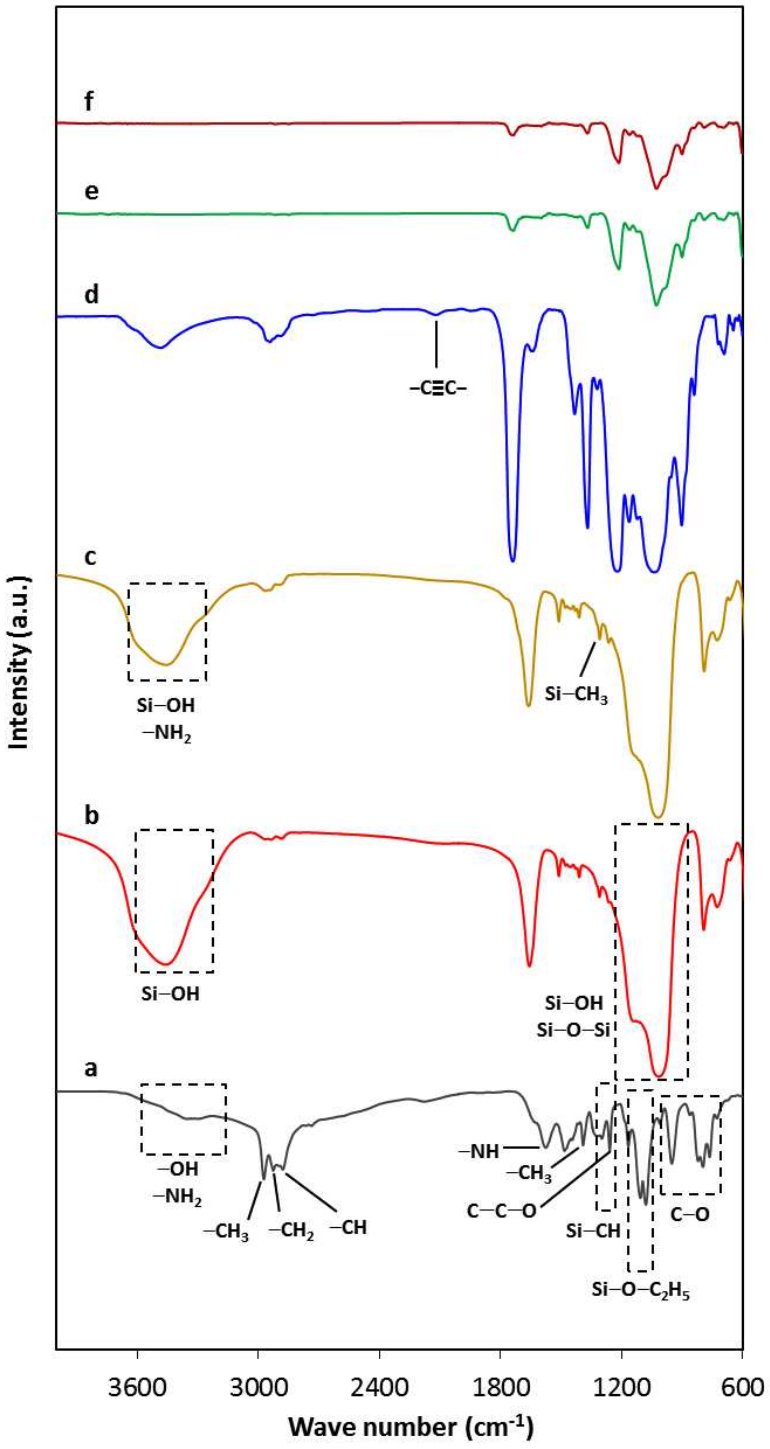

Figure 2. FTIR-ATR spectra of (a) the silane coupling agent (APDEMS), (b) NaY zeolite, (c) silylated NaY zeolite (NaY-sm), (d) neat CA membrane, (e) CA/NaY (20 wt.%), and (f) CA/NaY-sm (20 wt.%) mixed matrix membranes.

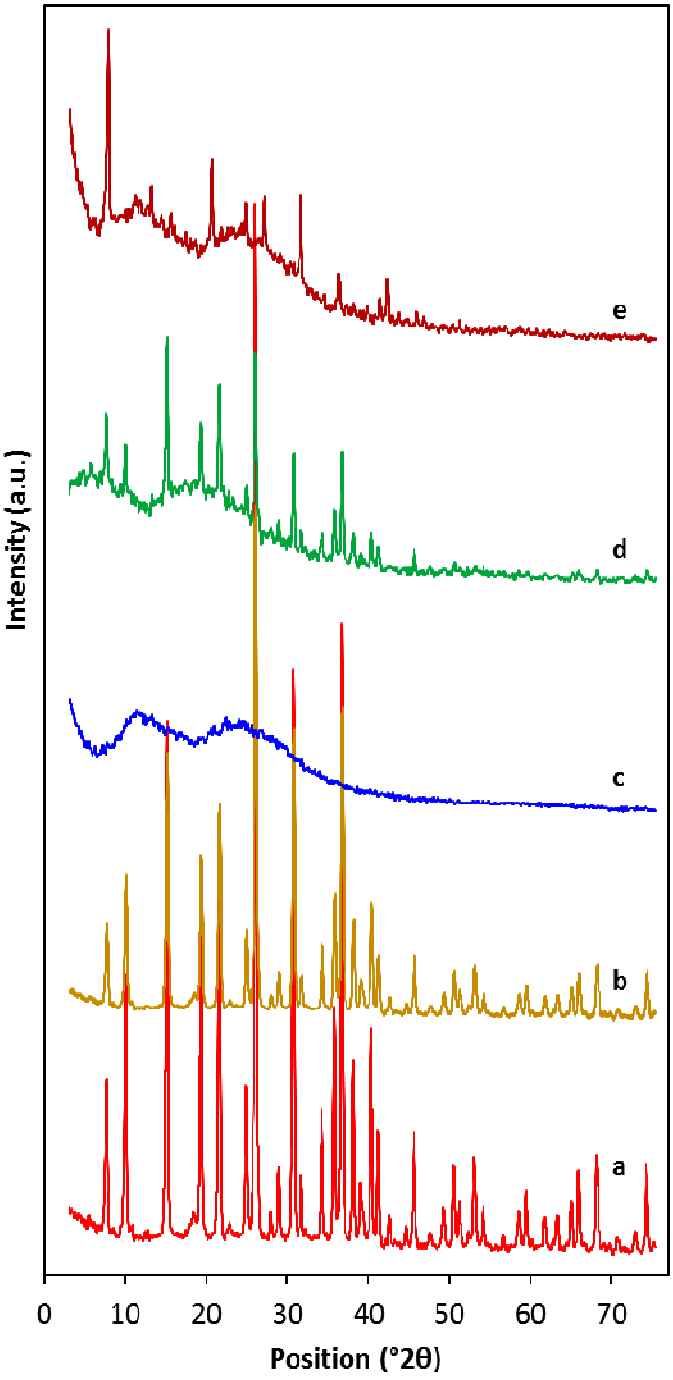

Figure 3. XRD patterns of (a) NaY zeolite, (b) silylated NaY zeolite (NaY-sm), (c) neat CA membrane, (d) CA/NaY (20 wt.%), and (e) CA/NaY-sm (20 wt.%) mixed matrix membranes.

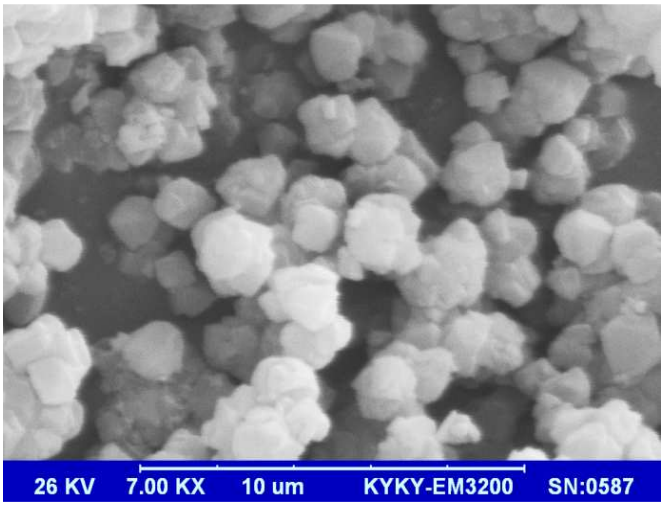

(a)

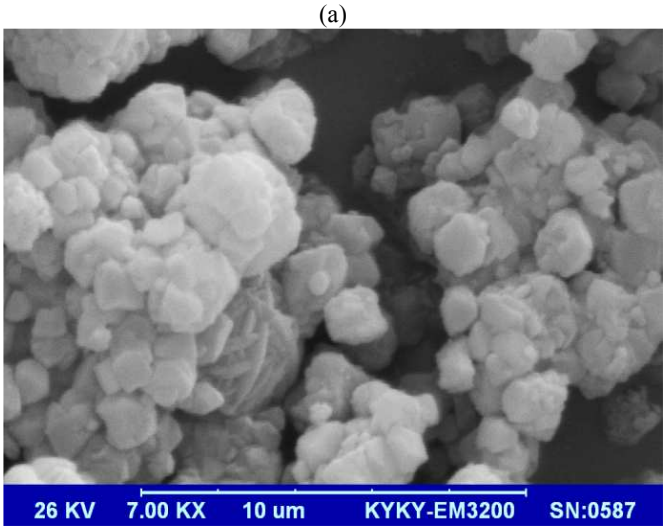

(b)

Figure 4. SEM images of (a) NaY and (b) NaY-sm powders.

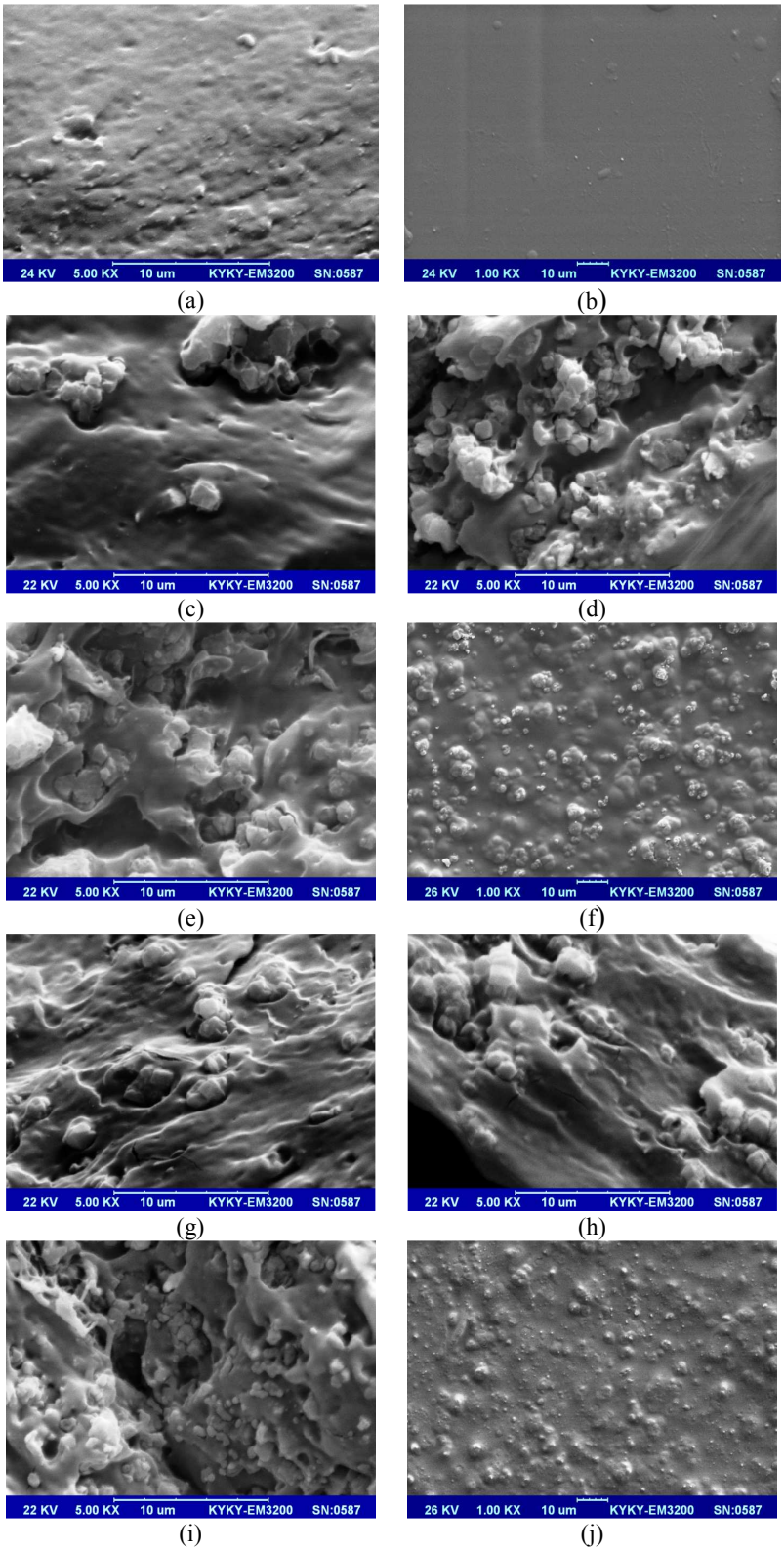

Figure 5. SEM images of the prepared membranes: (a) CA (cross), (b) CA (surface), (c) CA/NaY 5 wt.% (cross), (d) CA/NaY 20 wt.% (cross), (e) CA/NaY 25 wt.% (cross), (f) CA/NaY 20 wt.% (surface), (g) CA/NaY-sm 5 wt.% (cross), (h) CA/NaY-sm 20 wt.% (cross), (i) CA/NaY-sm 25 wt.% (cross), and (j) CA/NaY-sm 20 wt.% (surface).

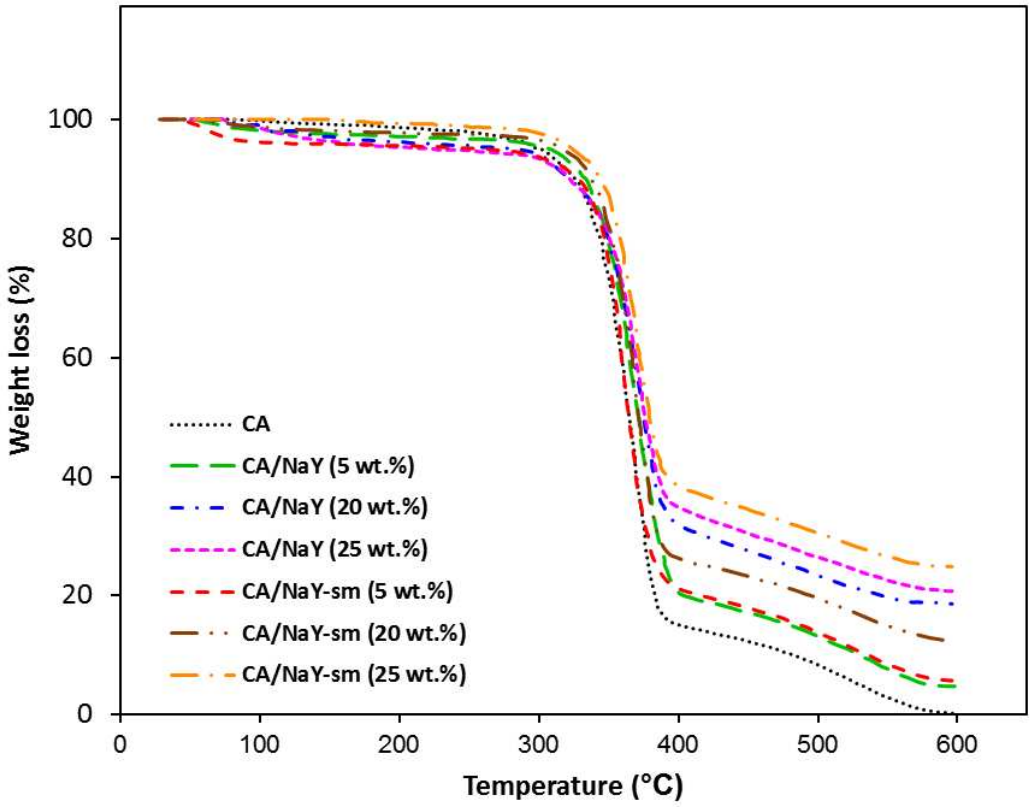

Figure 6. TGA spectra of the neat CA membrane and the related mixed matrix membranes containing NaY and NaY-sm zeolites.

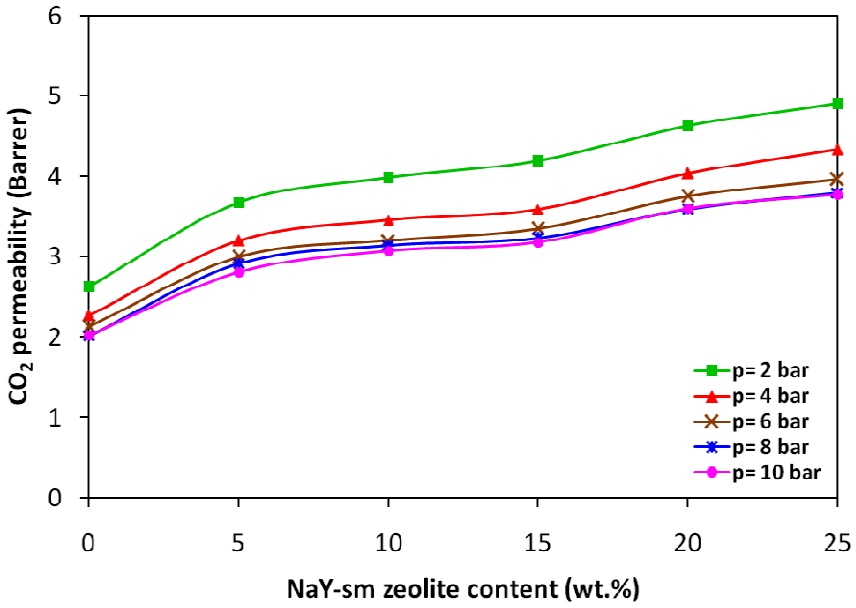

(a)

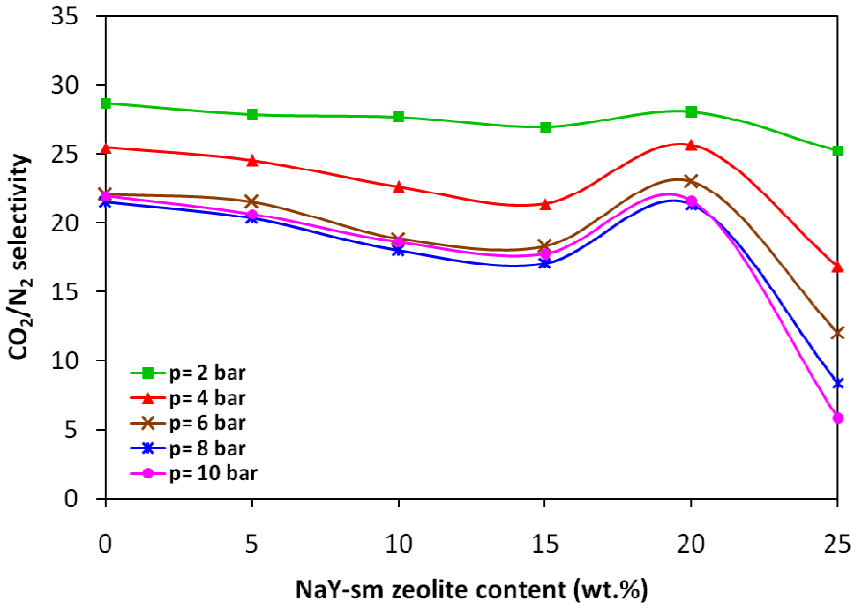

(b)

Figure 7. The effect of particle loadings on (a) CO_2 permeability and (b) CO_2/N_2 selectivity; the lines are only a guide to the eye.

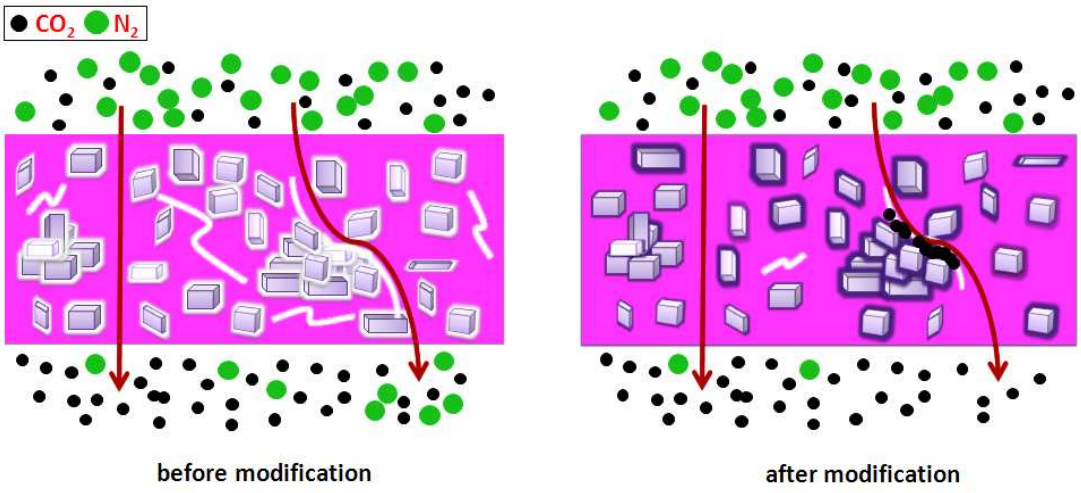

Figure 8. A schematic representation for CO_2/N_2 selectivity improvement via the facilitated CO_2 transport in the CA/NaY-sm membranes; the most widely used kinetic diameter was chosen for the effective molecular diameters of the penetrant gases which are respectively 3.3 and 3.64 Å for CO_2 and N_2 molecules.

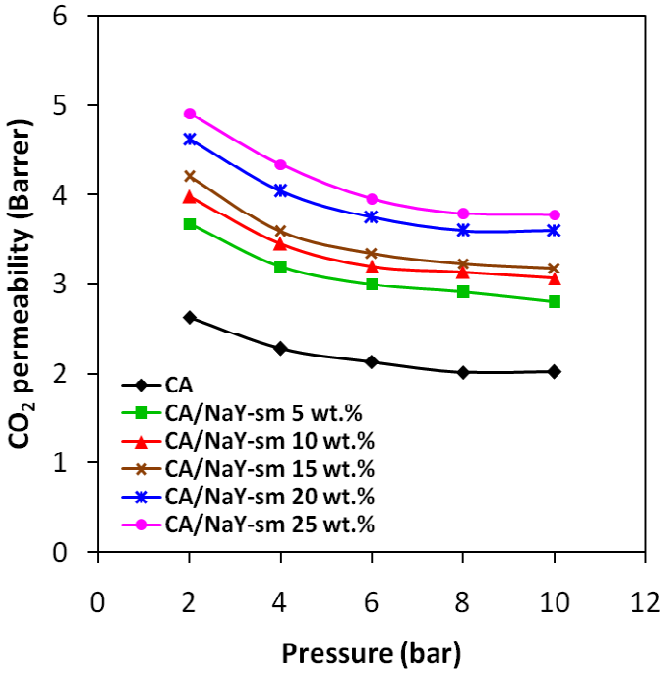

(a)

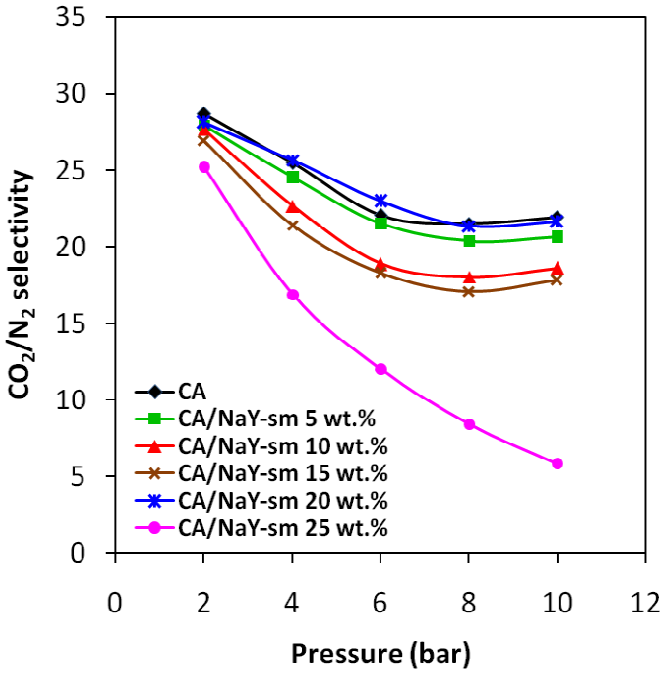

(b)

Figure 9. The effect of feed pressure on (a) CO_2 permeability and (b) CO_2/N_2 selectivity; solid lines are used only for connecting the data; the lines are only a guide to the eye.

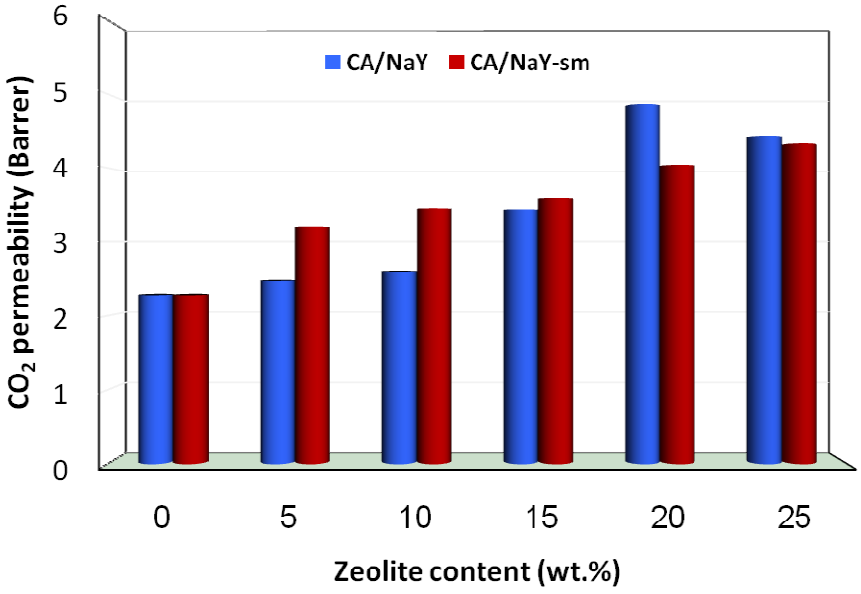

(a)

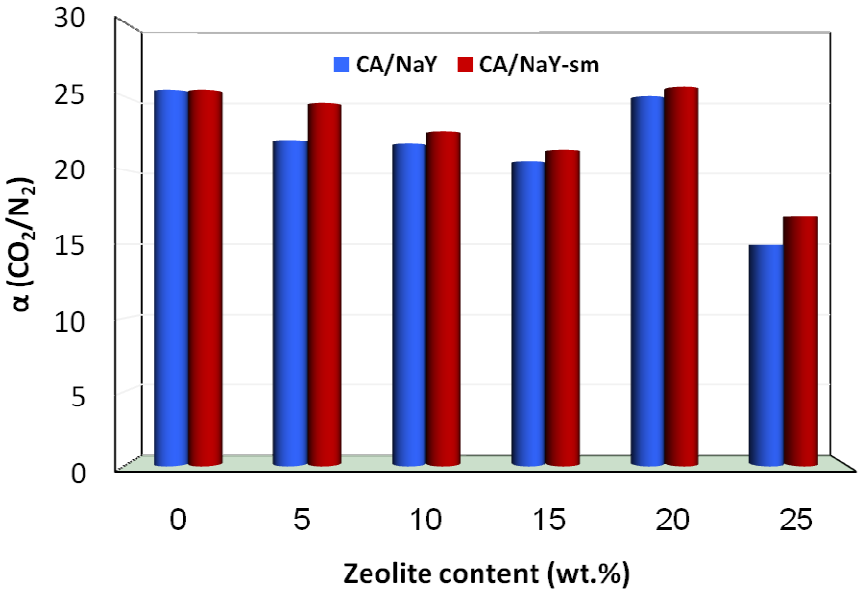

(b)

Figure 10. Comparing the performance of NaY and NaY-sm zeolites in the MMMs at 4 bar.

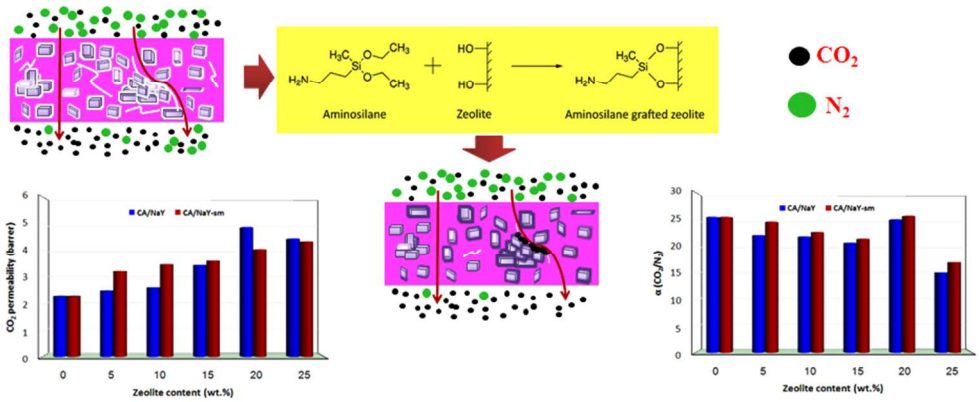

Graphical Abstract
252x108mm (96 x 96 DPI)